

TRANSFORMATION OF ZNO-BASED STRUCTURES UNDER HEAVY MO DOPING: DEFECT STATES AND LUMINESCENCE

¹Maksym BURYI, ¹Zdeněk REMEŠ, ^{1,2}Kateřina DĚCKÁ, ³Júlia MIČOVÁ, ^{1,4}Lucie LANDOVÁ

¹*Institute of Physics CAS in Prague, Prague, Czech Republic, EU, buryi@fzu.cz*

²*Czech Technical University in Prague, Faculty of Nuclear Sciences and Physical Engineering, Prague, Czech Republic, EU, katerina.decka@jfifi.cvut.cz*

³*Institute of Chemistry SAS, Bratislava, Slovakia, chemjumi@savba.sk*

⁴*Czech Technical University in Prague, Faculty of Electrical Engineering, Prague, Czech Republic, EU, abelova@fzu.cz*

<https://doi.org/10.37904/nanocon.2021.4321>

Abstract

Hydrothermally grown ZnO-based structures were heavily doped with Mo (various doping levels from 2 to 25%). Mo was found to strongly affect the structure and morphology of ZnO, resulting in a complex mixture of zinc oxide and molybdenum. Moreover, the transformation of material phases upon the increased Mo content was observed. ZnO phase was observed only at low Mo doping level (2 and 5%). This correlated very well to the changes in the luminescence and electron paramagnetic resonance signals.

Keywords: ZnO, Mo doping, material phase transformation, luminescence, electron paramagnetic resonance

1. INTRODUCTION

ZnO is a smart material which finds application in various fields of human activities: as scintillator, including application in time-of-flight positron emission tomography [1,2]; as electrode material in supercapacitors; in photocatalysis, energy harvesting and storage systems [3,4].

In majority of cases luminescence of ZnO nanostructures is composed of fast exciton luminescence peaks having maximum in near ultraviolet region at about 380 nm with decay time in the order of hundreds of ps and a relatively slow defects-related bands decay time in the order of tens of μ s. For example, the experimentally observed broad red bands ranging from 1 to 2 eV were related to zinc (V_{Zn}) or oxygen (V_O) vacancies [5]. The red emission bands (1.8-2 eV) related to V_{Zn} [5,6] were recently also observed in the hydrothermally grown ZnO nano- and microrods [7,8]. It is known that low-level Mo doping (below 1%) can positively affect the luminescence properties of ZnO (both defect-related and exciton luminescence) [7,8], whereas doping with 10 and 30% of Mo deteriorates them. Moreover, Mo has the tendency to couple with ZnO creating some new phase other than ZnO itself.

ZnO structure can also be characterized by the typical electron paramagnetic resonance (EPR) single-line signal observed at the g factor $g \approx 1.96$ ascribed to the shallow Ga, Al, H donors (SD) [9-12], the $Zn^+ + D$ complex, $D = Ga, Al, H$ [8]. The influence of Mo on this shallow donor was studied earlier [6,8] in the ZnO:Mo(0.05, 0.25, 1%) and ZnO:Mo(10, 30%).

However, there is no systematic investigation of the influence of Mo at the doping level within 2-25% on ZnO structure, morphology and creation of zinc-molybdenum complex oxides, luminescence and magnetic properties. Therefore, this is the aim of the present paper.

2. EXPERIMENTAL

2.1. Samples preparation

All reagents were analytical grade and were used as-received without further purification. Zinc nitrate hexahydrate ($\text{Zn}(\text{NO}_3)_2 \cdot 6\text{H}_2\text{O}$) and hexamethylenetetramine (HMTA, $\text{C}_6\text{H}_{12}\text{N}_4$) were purchased from Slavus and ammonium heptamolybdate tetrahydrate ($(\text{NH}_4)_6\text{Mo}_7\text{O}_{24} \cdot 4\text{H}_2\text{O}$ (NHMO) was obtained from Sigma-Aldrich. Deionized water was purified with a system So~Safe Water Technologies, having a conductivity $0.20 \mu\text{S} \cdot \text{cm}^{-1}$ at 25°C .

Undoped and Mo-doped ZnO nanorods with the Mo content 2-25% were prepared by the hydrothermal growth method. First, the corresponding stoichiometric amounts of $\text{Zn}(\text{NO}_3)_2 \cdot 6\text{H}_2\text{O}$ and $(\text{NH}_4)_6\text{Mo}_7\text{O}_{24} \cdot 4\text{H}_2\text{O}$, were dissolved in 200 ml and 50 ml of deionized water, respectively, with vigorous stirring by a magnetic stirrer. At the same time, a 25 mM aqueous solution of HMTA was prepared. All the solutions were filtered through a Whatman 2 filter. Subsequently, the filtered solutions were stirred vigorously for 15 min. The nominal concentration of the ZnO:Mo(2-25%) in the final suspensions was 25 mM. The solution of HMTA was added to the mixture. Stirring of the reaction mixture was followed by hydrothermal growth of nanorods by heating at 90°C for 3 hours. The grown nanorods were isolated and then purified (removal of residual salts), washing 5 times with deionized water and subsequent centrifugation at 18,000 rpm (RCF: 23,542 x g) for 15 minutes. Finally, the samples were lyophilized.

The amount of powder samples was approximately the same in all experiments.

2.2. Experimental techniques

XRD on powder samples was performed using RigakuMiniFlex 600 (Ni-filtered $\text{Cu-K}\alpha_{1,2}$ radiation) equipped with the NaI:Tl scintillation detector and XRD patterns were compared to the relevant records in the ICDD PDF-2 database (version 2013). The angular range was 10° - 80° , with a step of 0.02° and a scanning speed of $2^\circ/\text{min}$.

The size and morphology of ZnO NRs has been checked by scanning electron microscopy (SEM) using MAIA3, TESCAN electron microscope with the in-beam SE detector placed in objective lens and the electron beam energy 5 keV.

The steady-state photoluminescence (PL) spectra in the 350-800 nm spectral range were excited at frequency 333 Hz by pulsed 1 mW UV LED optically filtered by narrow band-pass filter centered at the wavelength 340 nm and recorded with 2 nm spectral resolution using the spectrally calibrated f/4 double gratings monochromator, long-pass filters, a red sensitive photomultiplier, current preamplifier ($10 \mu\text{A/V}$) and a lock-in amplifier referenced to the UV LED frequency. All PL spectra were spectrally calibrated, normalized at the wavelength 355 nm on the same value (dominated by optical scattering of excitation light) and converted from wavelength to energy scale taking into account the Jacobian correction [13]. PL spectra were measured with 5 mg ZnO powder pressed in a Suprasil glass tube with the inner (outer) diameter 2 mm (3 mm) featuring a low fluorescence background.

EPR measurements were performed with a commercial Bruker EMXplus spectrometer in the X-band (9.4 GHz) within the 4-296 K temperature range using Oxford Instruments ESR900 cryostat. The spectrometer sensitivity is about 10^{12} spins/mT.

3. RESULTS AND DISCUSSION

3.1. Phase purity and morphology

The XRD patterns of ZnO:Mo(2-25%) samples are demonstrated in **Figure 1**.

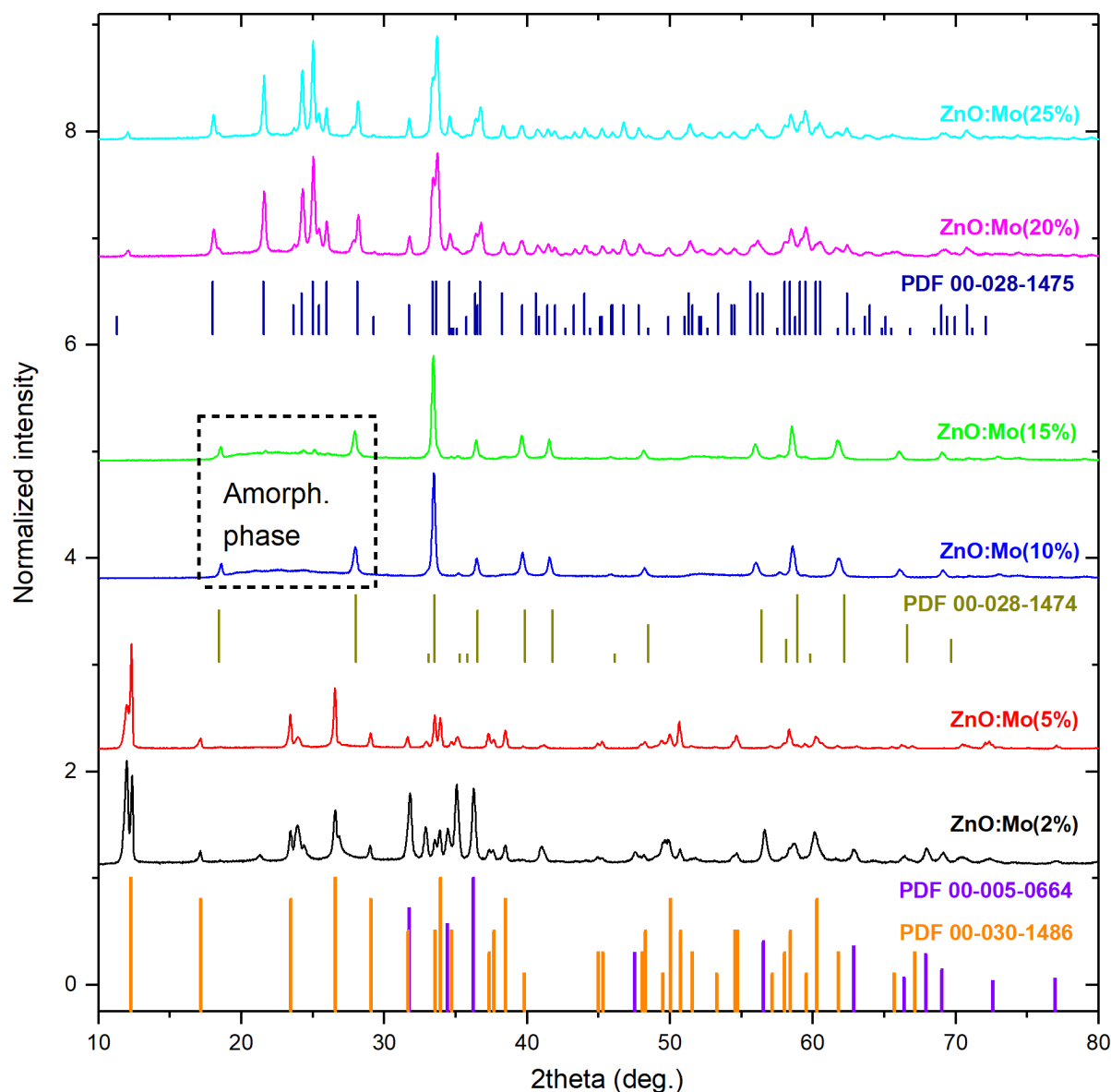


Figure 1 XRD patterns of the ZnO:Mo(2-25%). The positions of the XRD reflections are indicated by vertical solid lines distinguished by color according to the corresponding record in the ICDD PDF-2 database: PDF 00-005-0664 (hexagonal ZnO), PDF 00-030-1486 ($\text{Zn}_5\text{Mo}_2\text{O}_{11}\cdot 5\text{H}_2\text{O}$), PDF 00-028-1474 ($\text{MoO}_3\cdot 2\text{ZnO}\cdot \text{H}_2\text{O}$), PDF 00-028-1475 ($2\text{MoO}_3\cdot 3\text{ZnO}\cdot \text{H}_2\text{O}$).

The XRD patterns of ZnO:Mo(2-25%) are very complex, especially at the largest Mo content, composed of different material phases (they were tentatively ascribed to the complex zinc-molybdenum oxides). The negligibly small presence of ZnO phase could be detected only in the ZnO:Mo(2, 5%) dominated by some other material phase. This phase was tentatively ascribed to $\text{Zn}_5\text{Mo}_2\text{O}_{11}\cdot 5\text{H}_2\text{O}$. Further increase of the Mo content to 10 and 15% resulted in the disappearance of the ZnO phase and transformation of the $\text{Zn}_5\text{Mo}_2\text{O}_{11}\cdot 5\text{H}_2\text{O}$ to the $\text{MoO}_3\cdot 2\text{ZnO}\cdot \text{H}_2\text{O}$. Moreover, some unknown amorphous phase appeared. Its origin is unknown. Further increase of the Mo content to 20 and 25% results in the $\text{MoO}_3\cdot 2\text{ZnO}\cdot \text{H}_2\text{O}$ transformation into the $2\text{MoO}_3\cdot 3\text{ZnO}\cdot \text{H}_2\text{O}$ while amorphous phase disappeared.

SEM provides an insight into the morphology of the ZnO:Mo(2-25%) samples. The corresponding images are shown in **Figure 2**. The ZnO:Mo(2%) sample is the only consisting of hexagonal prismoid microrods, in average, of the size 1-2 μm in circumference and over 3 μm long (**Figure 2A**). However, the microrods are

outnumbered by the irregular flat slab-like structures with the averaged area of about $1\text{-}10\ \mu\text{m}^2$. Interestingly, the ZnO:Mo(5%) sample is composed of hexagons, varying in “diameter” within the $5\text{-}10\ \mu\text{m}$ range and about $0.5\ \mu\text{m}$ thick (**Figure 2B**).

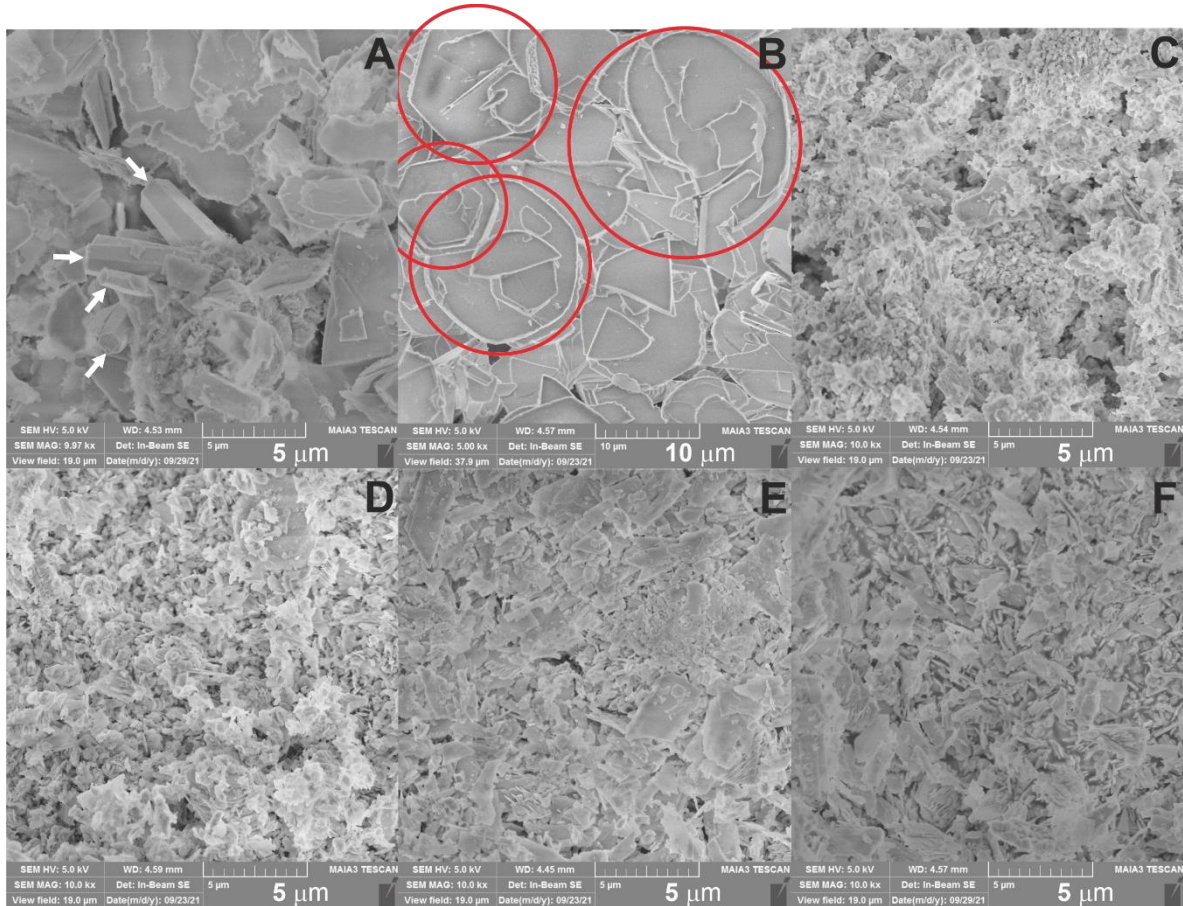


Figure 2 SEM images of the ZnO:Mo(2-25%) samples with different magnification as indicated in Figures: A – ZnO:Mo(2%); B - ZnO:Mo(5%); C - ZnO:Mo(10%); D - ZnO:Mo(15%); E - ZnO:Mo(20%); F - ZnO:Mo(25%). ZnO microrods are stressed by white arrows. Hexagons are marked by red circles.

The ZnO:Mo(10-25%) samples consist of flake-like sheared structures with the averaged area about $0.25\ \mu\text{m}^2$ (**Figures 2C-F**). In the ZnO:Mo(20, 25%) samples the flakes are getting mixed with the larger slabs of the averaged area of about $5\ \mu\text{m}^2$. This is consistent with the previous study of the ZnO:Mo(30%) [7].

Based on the XRD and SEM analyses one may conclude that the increased Mo doping level results in the phase transformation and changes in morphology of the ZnO:Mo(2-25%) samples.

3.2. PL and EPR characterization

PL spectra have been measured in all the ZnO:Mo(2-25%) samples at room temperature as can be seen in **Figure 3A**. The spectrum of ZnO:Mo(2%) is composed of two very broad overlapped bands (B1 (~2.14 eV) and B3(~2.80 eV)) – covering the 1.4-3.4 eV energy region. Surprisingly, the PL spectrum of the ZnO:Mo(5%) is single-band peaking at 2.64 eV (B2 band with 1 eV full width at half maximum (FWHM)). Furthermore, the B2 band is getting weaker upon the increased Mo content to 10 and 15% and the new clearly visible very narrow bands appear (B4-7 peaking at 2.96, 3.16, 3.24 and 3.34 eV, respectively). The B4-7 bands may be ascribed to exciton-like emission observed in ZnO [14], especially considering the existence of ZnO part in the complex zinc-molybdenum oxide creating ZnO:Mo(10, 15%) samples as discussed in the subsection above

(see also **Figure 1**). The B4-7 bands are weaker in the ZnO:Mo(15%) sample. The new single-band spectra, B3' (~2.91 eV), of the same amplitude are observed in the ZnO:Mo(20, 25%) samples. All of this confirms the gradual phase transformation upon the increased Mo content in the ZnO:Mo(2-25%) samples.

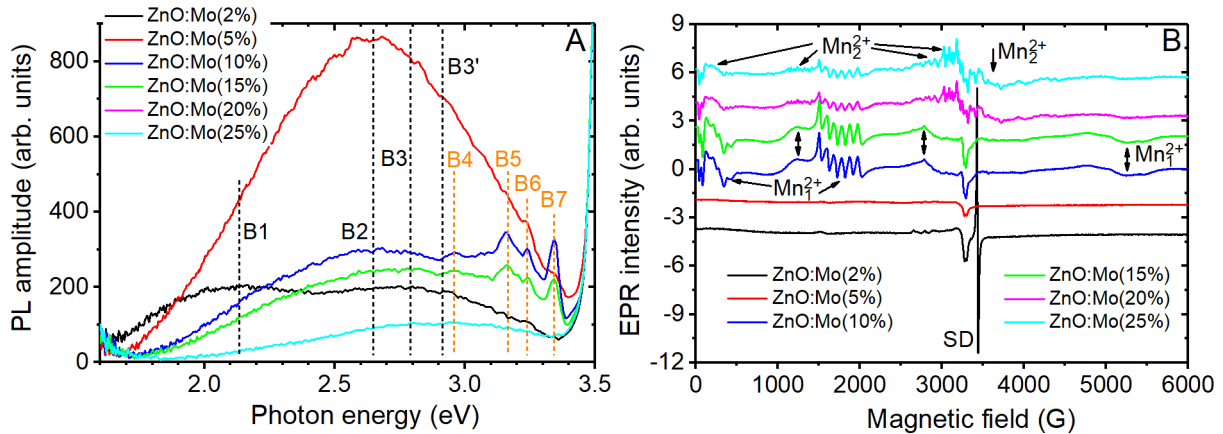


Figure 3 A - PL spectra measured in the ZnO:Mo(2-25%). B1-3,3',4-7 indicate specific emission bands. The signal above 3.4 eV is scattered light. **B** – EPR spectra measured in the ZnO:Mo(2-25%). “SD” stands for “shallow donors”. Mn_{1,2}²⁺ and vertical double arrows indicate the spectra of two different Mn²⁺ centers.

In order to find out the presence of paramagnetic centers and their evolution upon the increased Mo content, EPR spectra were measured in all the ZnO:Mo(2-25%) samples and shown in **Figure 3B**. Only the spectrum of the ZnO:Mo(2%) was attributed with the SD signal at the g factor $g = 1.954$. The rest of visible signals were not identified. This signal is absent in the spectrum of the ZnO:Mo(5%). Based on this fact and considering also the XRD results above, one may conclude that only the tiniest amount of ZnO phase exists in the ZnO:Mo(5%) sample. The SD signal is absent in the EPR spectra of the ZnO:Mo(10, 15%). However, there are some resonances which were identified as belonging to Mn²⁺ (electron spin $S = 5/2$ and the ⁵⁵Mn nucleus with 100% abundance and nuclear spin $I = 5/2$), Mn₁²⁺ – there are five components due to $S = 5/2$ with the one exhibiting the most pronounced hyperfine structure (sextet of lines because of $I = 5/2$ with the center at 1738 G) [15]. The Mn₁²⁺ spectrum is getting weaker in the ZnO:Mo(20, 25%) samples, and the new Mn²⁺ spectrum appears (Mn₂²⁺). It was identified using similar consideration as for the Mn₁²⁺ identification above. The Mn²⁺ is an accidental impurity but serves as a good indicator of the gradual material phase transformation. The SD signal is absent in the EPR spectra of the ZnO:Mo(20, 25%) as well. This correlates well to the XRD and PL measurements above.

4. CONCLUSION

It has been found that heavily Mo-doped hydrothermally grown ZnO-based structures appear a mix of different zinc-molybdenum complex oxides upon the increased Mo content. Their morphology is changing upon the Mo doping level from microrods to microhexagons, then to micro- and nanoflakes and microslabs as well. This is confirmed by the observed transformations of PL and EPR spectra.

ACKNOWLEDGEMENTS

This work was supported by the Czech Science Foundation by the project No. 20-05497Y, CAS Mobility Plus project SAV-AV CR-21-09 and by the Scientific Grant Agency of Ministry of Education, Science, Research and Sport of Slovak Republic and Slovak Academy of Sciences (VEGA 2/0157/20).

REFERENCES

- [1] LEITER, F., ZHOU, H., HENECKER, F., HOFSTAETTER, A., HOFMANN, D. M., MEYER, B. K. Magnetic resonance experiments on the green emission in undoped ZnO crystals, *Physica B*. 2001, vol. 308–310, pp. 908–911.
- [2] LECOQ, P. Pushing the Limits in Time-of-Flight PET Imaging, *IEEE Trans. Radiat. Plasma Med. Sci.* 2017, vol. 1, pp. 473–485.
- [3] NAJIB, S., BAKAN, F., ABDULLAYEVA, N., BAHARIQUSHCHI, R., KASAP, S., FRANZÒ, G., SANKIR, M., SANKIR, N. D., MIRABELLAD, S., ERDEM, E. Tailoring morphology to control defect structures in ZnO electrodes for high-performance supercapacitor devices, *Nanoscale*. 2020, vol. 12, pp. 16162-16172.
- [4] TOUFANI, M., KASAP, S., TUFANI, A., BAKAN, F., WEBER, S., ERDEM, E. Synergy of nano-ZnO and 3D-graphene foam electrodes for asymmetric supercapacitor devices, *Nanoscale*. 2020, vol. 12, pp. 12790-12800.
- [5] FRODASON, Y. K., JOHANSEN, K. M., BJØRHEIM, T. S., SVENSSON, B. G., ALKAUSKAS, A. Zn vacancy as a polaronic hole trap in ZnO. *Phys. Rev. B*. 2017, vol. 95, 094105.
- [6] BURYI, M., REMEŠ, Z., BABIN, V., ARTEMENKO, A., VANĚČEK, V., AUBRECHTOVÁ DRAGOUNOVÁ, K., LANDOVÁ, L., KUČERKOVÁ, R., MIČOVÁ, J. Transformation of free-standing ZnO nanorods upon Er doping, *Applied Surface Science*. 2021, vol. 562, 150217.
- [7] BURYI, M., REMEŠ, Z., BABIN, V., VANĚČEK, V., AUBRECHTOVÁ DRAGOUNOVÁ, K., MIČOVÁ, J., LANDOVÁ, L., KUČERKOVÁ, R. ZnO nanorods alloyed with Mo/Er. The effect of postdeposition treatment on defect states and luminescence. *IOP Conf. Ser.: Mater. Sci. Eng.* 2021, vol. 1050, 012002.
- [8] BURYI, M., REMEŠ, Z., BABIN, V., NOVOTNÝ, M., VANĚČEK, V., AUBRECHTOVÁ DRAGOUNOVÁ, K., MIČOVÁ, J., LANDOVÁ, L., KUČERKOVÁ, R., MORE-CHEVALIER, J., CHERTOPALOV, S., FITL, P., KMJEČ, T. Influence of Mo doping on the luminescence properties and defect states in ZnO nanorods. Comparison with ZnO:Mo thin films, *Applied Surface Science*. 2021, vol. 555, 149679.
- [9] JANOTTI, A., VAN DE WALLE, CH. G. Native point defects in ZnO. *Phys. Rev. B*. 2007, vol. 76, 165202.
- [10] JANOTTI, A., VAN DE WALLE, CH. G. Fundamentals of zinc oxide as a semiconductor. *Rep. Prog. Phys.* 2009, vol. 72, 126501.
- [11] GONZALES, C., BLOCK, D., COX, R. T., HERVÉ, A. Magnetic resonance studies of shallow donors in zinc oxide. *J. Crystal Growth* 1982, vol. 59, 357.
- [12] BLOCK, D., HERVÉ, A., COX, R. T. Optically detected magnetic resonance and optically detected ENDOR of shallow indium donors in ZnO. *Phys. Rev. B* 1982, vol. 25, 6049.
- [13] MOONEY, J., KAMBHAMPATI, P. Get the Basics Right: Jacobian Conversion of Wavelength and Energy Scales for Quantitative Analysis of Emission Spectra. *J. Phys. Chem. Lett.* 2013, vol. 4, pp. 3316–3318.
- [14] ÖZGÜR, Ü., ALIVOV, YA. I., LIU, C., TEKE, A., RESHCHIKOV, M. A., DOĞAN, S., AVRUTIN, V., CHO, S.-J., MORKOÇ, H. A comprehensive review of ZnO materials and devices. *J. Appl. Phys.* 2005, vol. 98, 041301.
- [15] ABRAGAM, A., BLEANEY, B. *Electron Paramagnetic Resonance of Transition Ions*. Oxford: Clarendon Press, 1970, vol. 1.